




Article

# Effects of Additives on Electrochromic Properties of Nanocrystalline Tungsten Oxide Films Prepared by Complexation-Assisted Sol–Gel Method

Dan Zhou , Zhibo Tong , Hongmei Xie, Jiaotong Sun and Fenggui Chen 

Chongqing Key Laboratory of Extraordinary Bond Engineering and Advanced Materials Technology, College of Materials Science and Engineering, Yangtze Normal University, Chongqing 408100, China

\* Correspondence: zhoudan@yznu.edu.cn; Tel.: +86-023-72791828

**Abstract:** To improve the electrochromic (EC) properties of sol–gel-derived WO<sub>3</sub> films, a series of organic small molecules, such as dopamine (DA), catechol, tyramine, phenol and 2-phenylethylamine, were added into peroxotungstic acid precursor sols as structure-directing additives, and five modified WO<sub>3</sub> films were prepared by a simple and low-cost complexation-assisted sol–gel method. The effects of the above additives on the EC properties of the modified WO<sub>3</sub> films have been studied in detail. Compared with the pure WO<sub>3</sub> polycrystalline film, all the modified films combine the advantages of nanocrystalline and amorphous phases and show higher EC properties attributed to the unique nanocrystal-embedded amorphous structure. The results indicate that different additives with different numbers and types of functional groups (hydroxyl and amino groups) can change the microstructure, morphology, and thus electrochemical and EC properties of the films in various degrees. The additives, in order of their strong interactions with the sols, are DA, catechol, tyramine, phenol and 2-phenylethylamine, primarily depending on the number of hydroxyl groups. Of all the additives, DA with both catechol hydroxyl and amino groups shows the most positive effect; that is, the WO<sub>3</sub> film modified with DA exhibits the best EC properties in terms of contrast, switching speed, stability, and coloration efficiency.



**Citation:** Zhou, D.; Tong, Z.; Xie, H.; Sun, J.; Chen, F. Effects of Additives on Electrochromic Properties of Nanocrystalline Tungsten Oxide Films Prepared by Complexation-Assisted Sol–Gel Method. *Materials* **2023**, *16*, 2681. <https://doi.org/10.3390/ma16072681>

Academic Editors: Verónica de Zea Bermudez and Mariana Fernandes

Received: 5 March 2023

Revised: 21 March 2023

Accepted: 26 March 2023

Published: 28 March 2023



**Copyright:** © 2023 by the authors. Licensee MDPI, Basel, Switzerland. This article is an open access article distributed under the terms and conditions of the Creative Commons Attribution (CC BY) license (<https://creativecommons.org/licenses/by/4.0/>).

**Keywords:** tungsten oxide; nanocrystalline; electrochromic property; additive; complexation; sol–gel method; film

## 1. Introduction

In recent years, under the background of sustainable development, the electrochromic (EC) smart window has been considered as a promising energy-conservation and emission-reduction device for green buildings, vehicles, etc. and received more and more attention [1,2]. EC materials, the most important component of a smart window, can change their optical properties (absorption, reflectance, transmittance, etc.) reversibly under a small applied voltage, and they have also been widely applied to energy-saving displays and antiglare automobile rear-view mirrors, in addition to smart windows, which are thought to be one of the most potential green energy-saving materials [3–5].

Transition metal oxides are commonly used as EC materials [3,5,6]. Among them, tungsten oxide (WO<sub>3</sub>) is the most studied and extremely attractive one due to its high transmittance contrast, thermal and photo stability, good ionic and electronic conductivity, and improved lifetime of the devices. Many techniques can be used to prepare WO<sub>3</sub> EC films, including chemical vapor deposition (CVD) [7], sputtering [8], evaporation [9] and so on. However, the WO<sub>3</sub> films produced by the above methods are expensive and inefficient because of the special equipment and high vacuum conditions, impeding their commercial applications. Therefore, the sol–gel method [10–12], a wet-chemical route, is attractive and regarded as an alternative owing to its low cost, simplicity, repeatable process, and uniform and large-area film formation. Moreover, during the sol–gel process, the microstructure,

crystal size, porosity and composition of the deposited films can be easily controlled by optimizing various preparation parameters or introducing additives into the sols [13], which will affect the kinetics, durability and coloration efficiency of the thin films [14].

The EC performances of the WO<sub>3</sub> films prepared by the traditional sol–gel method, however, are still not good enough for actual use, such as inadequate optical contrast, switching time, long-term electrochemical cycling stability or coloration efficiency. Many researchers have tried to adjust and control the structures/morphology of the sol–gel-derived WO<sub>3</sub> films by using organic additives to improve their EC performances. Research works can be mainly divided into two categories: one is to add pore-forming templates (polymers or surfactants) into the sol and then remove the templates through heat treatment or solvent extraction [15–18]. The obtained high-porosity WO<sub>3</sub> films possess a very large specific surface area, which can increase the color response speed and optical contrast. However, the stability of the high-porosity structure decreases [19], because part of the structure is easily destroyed or collapsed during the heat treatment process or the surface erosion rate is accelerated during the electrochemical cycling test. The other is to add a large amount of alcohols, organic acids or other organic compounds into the precursor sols to increase the contrast and switching speed [20,21]. Unfortunately, this kind of method cannot effectively enhance the combination property of the films and may bring some environmental and health problems. Therefore, it is highly desirable to develop sol–gel-derived WO<sub>3</sub> EC films with excellent optical contrast, switching time, cycling stability, and coloration efficiency satisfying practical requirements.

It has been demonstrated that the EC properties of the films are greatly affected by the structure and morphology. It is well known that an amorphous WO<sub>3</sub> film is characterized by a short switching time, high coloration efficiency and high contrast due to its loose structure and large surface area [13,18,21]. However, because an amorphous film has many structural defects, the electrochemical properties of the film will irreversibly deteriorate during the EC cycling. On the other hand, a highly crystalline WO<sub>3</sub> film shows high electrochemical stability owing to its compact and ordered structure, but it may be too dense for ions diffusion and intercalation, leading to a slow response time or low contrast. A number of efforts have been undertaken to overcome the problems and combine the advantages of the two structures in nanoscale [22].

In our previous work, a complexation-assisted sol–gel method was proposed in order to improve the EC properties of traditional sol–gel-derived WO<sub>3</sub> films, in which a small amount of dopamine (DA) was added into peroxotungstic acid (PTA) precursor sol to produce PTA–DA complex sol [23]. The DA molecules suppressed the formation of very large WO<sub>3</sub> particles in the precursor sol and inhibited the formation of a highly stressed polycrystalline structure during annealing. The DA-modified WO<sub>3</sub> films exhibited much higher optical contrast, coloration efficiency, switching speed, and excellent long-term cycling stability (up to 35,000 cycles) than the pure WO<sub>3</sub> film due to nanocrystal surrounded by amorphous matrix.

So far, however, very little work has been completed to investigate the function of different additives or complexing agents during the preparation and application of the sol–gel-derived WO<sub>3</sub> films in detail. In this paper, therefore, a series of organic small molecules, such as DA, catechol (CA), tyramine (TA), phenol (Ph) and 2-phenylethylamine (PEA), are added into PTA precursor sol as structure-directing additives, and a variety of modified WO<sub>3</sub> films are prepared by a simple and low-cost complexation-assisted sol–gel method to study the effects of the above additives containing different numbers and types of functional groups (hydroxyl and amino groups) on the structure, morphology, electrochemical and EC properties of the modified WO<sub>3</sub> films.

## 2. Materials and Methods

### 2.1. Materials

DA hydrochloride (98%), CA (99%), TA hydrochloride (98%), Ph ( $\geq 99\%$ ), PEA hydrochloride (98%), 30% H<sub>2</sub>O<sub>2</sub>, lithium perchlorate (LiClO<sub>4</sub>) (99.9%), propylene carbonate

(PC) ( $\geq 98\%$ ), acetone (98%) and isopropanol (99%) were obtained from Shanghai Aladdin Chemical Reagent Co., Ltd. (Shanghai, China). Tungsten powder ( $\geq 99\%$ ) was received from Merck KGaA (Darmstadt, Germany). Conducting indium tin oxide-coated glass (ITO glass,  $< 7 \Omega/\square$ ) was purchased from Zhuhai Kaivo Optoelectronic Technologies Co. (Zhuhai, China).

## 2.2. Preparation of the Modified $WO_3$ Films

Prior to use, the ITO glass was cleaned with detergent, deionized  $H_2O$ , acetone, and isopropanol for 10 min in an ultrasonic bath, respectively. Then, the ITO glass was further cleaned by a plasma treatment for 5 min to improve their hydrophilicity.

The modified  $WO_3$  films were produced through our previous complexation-assisted sol-gel method [23] with slight modification. First, 20 mmol tungsten powder was added in 60 mL 30%  $H_2O_2$  solution at  $0^\circ C$  under continuously magnetic stirring to form a colorless transparent PTA, which was followed by a reflux at  $60^\circ C$  for 6 h to decompose of excess peroxide. After slow stirring for one week, 3.3 mmol DA was introduced into the PTA sol to obtain concentrated yellow PTA/DA complex sol after heating at  $60^\circ C$  for 10 h. The PTA/DA sol was coated on the cleaned ITO glass by spin-coating technology, and the as-prepared film was dried at  $60^\circ C$  for 1 h followed by annealing at  $300^\circ C$  for 2 h to form the modified  $WO_3/DA$  film. The film thickness was controlled at about 200 nm. Meanwhile, other modified  $WO_3$  films by adding CA, TA, Ph, and PEA were prepared in the same way, respectively. The as-prepared films are denoted as  $WO_3/DA-300^\circ C$ ,  $WO_3/CA-300^\circ C$ ,  $WO_3/TA-300^\circ C$ ,  $WO_3/Ph-300^\circ C$ , and  $WO_3/PEA-300^\circ C$ , respectively. For comparison, the pure  $WO_3-300^\circ C$  film was also prepared under the similar conditions except in the absence of additives.

For Fourier transform infrared spectroscopy (FTIR) characterization, xerogel samples were obtained by drying the PTA and PTA/additive complex sols in vacuum oven at  $60^\circ C$  for 24 h and marked as  $WO_3$ ,  $WO_3/DA$ ,  $WO_3/CA$ ,  $WO_3/TA$ ,  $WO_3/Ph$  and  $WO_3/PEA$  xerogels, respectively.

## 2.3. Characterization of the Modified $WO_3$ Films

The UV-Vis absorption spectra (400–800 nm) of various sols and films were obtained on a UV-VIS-NIR spectrophotometer (Shimadzu UV-3600, Tokyo, Japan). The FTIR spectra of the xerogels and films from 400 to  $4000\text{ cm}^{-1}$  were recorded on a Nicolet is5 FTIR spectrometer (Thermo Fisher Scientific, Waltham, MA, USA). The morphology and microstructure of the films were observed by a field-emission scanning electron microscope (FESEM, ZEISS GeminiSEM 300, Oberkochen, Germany) and a transmission electron microscope (TEM, JEOL-2100F, Tokyo, Japan). X-ray diffraction (XRD) analyses of all the samples were characterized by a Shimadzu XRD-6100 diffractometer with an X-ray wavelength of  $1.542\text{ \AA}$  (Cu  $K\alpha$  radiation, 40 kV and 30 mA) over a 2-theta range of  $10\text{--}60^\circ$ .

## 2.4. Measurement of Electrochemical and EC Properties

The electrochemical properties of the films were tested using a three-electrode system with  $LiClO_4/PC$  (1 mol/L) as a electrolyte, Pt sheet as a counter-electrode, Ag/AgCl as a reference electrode, and the prepared films coated on ITO glass as working electrodes. Nyquist plots of the films were performed using an AUTOLAB PGSTAT 302N potentiostat/galvanostat analyzer (Eco Chemie) at a perturbation voltage of 10 mV in the frequency range of 10 kHz to 10 mHz. Cyclic voltammetry (CV) plots were collected on an AUTOLAB analyzer at a scan rate of  $100\text{ mV s}^{-1}$  from  $-1.0$  to  $+1.0$  V, and all current densities were normalized to the geometric surface area of the electrodes.

EC properties (visible spectra (400–800 nm) and dynamic switching curves at 720 nm) of the films were recorded on a Shimadzu UV-3600 spectrophotometer in combination with an AUTOLAB analyzer by applying constant potentials and square-wave potentials (oscillating between  $+1.0$  V and  $-1.0$  V at a time step of 50 s), respectively.

### 3. Results and Discussion

#### 3.1. Preparation and Characterization of the Modified WO<sub>3</sub> Films

In order to study the effects of the additives, that is, different numbers and types of functional groups (hydroxyl and amino groups), on the structure, morphology, electrochemical and EC properties of WO<sub>3</sub> films prepared by the sol–gel method, DA, CA, TA, Ph, and PEA were selected as additives and added into the PTA precursor sols to produce a variety of modified WO<sub>3</sub> films. Figure 1 displays the structural formulas of these five additives or their hydrochlorides. DA contains both catechol hydroxyl and amino functional groups in which the catechol units are well known to show quite strong affinity to various kinds of metals/metal ions [24], and the amino groups are mainly in the form of ammonium salt. The catechol hydroxyl groups of DA can bind uncoordinated tungsten atoms on the surface of PTA colloid nanoparticles strongly via the deprotonated O, O' sites [25–27] in monodentate, bidentate, or chelated modes [28]. There is also the possibility of hydrogen bonding between the hydroxyl groups on DA and O atoms on PTA. CA has catechol hydroxyl groups and no amino group. TA possesses one hydroxyl group and one amino group. Meanwhile, both Ph and PEA are monofunctional compounds, containing only one hydroxyl group and one amino group, respectively.

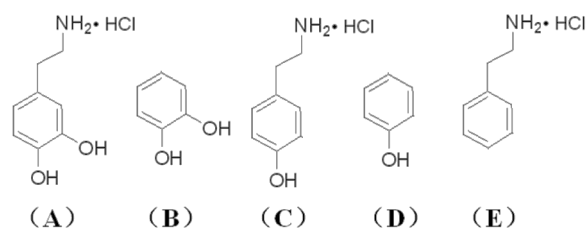


**Figure 1.** Structural formulas of (A) DA hydrochloride, (B) CA, (C) TA hydrochloride, (D) Ph and (E) PEA hydrochloride.

A nearly colorless and transparent PTA sol was formed after one-week stirring of the reactive mixture of tungsten powder and H<sub>2</sub>O<sub>2</sub>, as shown in the photo of the inset of Figure 2. When the additives were introduced into the sols, respectively, the color of the complex sols immediately darkened significantly (inset of Figure 2), indicating an instantaneous formation of charge-transfer complexes due to the strong complexation, hydrogen bonding, or electrostatic interaction between the functional groups of the additives and tungsten or oxygen atoms of PTA colloidal nanoparticles. Furthermore, as can be seen from Figure 2, UV-Vis absorption spectra of these complex sols show a red-shift and enhanced intensity compared with that of the pure PTA sol, which is similar to the phenomenon observed from DA-TiO<sub>2</sub> complexes [29,30].

To prove the successful preparation of the complex sols and study the interactions between the PTA sol and the additives, all the PTA and complex sols were dried in a vacuum oven at 60 °C for 24 h to form xerogels, and the FTIR spectra of the xerogels are compared in Figure 3A. As can be seen from Curve a of Figure 3A, the broad absorption band of the pure WO<sub>3</sub> xerogel at wavenumbers around 3500 cm<sup>-1</sup> is caused by the stretching vibration  $\nu(\text{OH})$  of water and hydroxyl adsorbed or incorporated in the xerogel, and the peak at 1629 cm<sup>-1</sup> can be attributed to the in-plane bending vibration  $\delta(\text{HOH})$  of water molecules [31]. In addition, the pure WO<sub>3</sub> xerogel shows key characteristic absorption bands of amorphous WO<sub>3</sub>, for example, the peaks corresponding to the stretching vibration of terminal W=O bonds (975 cm<sup>-1</sup>) on the surface of the nanoparticles and micro-voids of the xerosol [32], the stretching vibration of bridging peroxide W–O–W (882 cm<sup>-1</sup>), the W–O–W bridging mode of the W–O<sub>6</sub> corner-sharing octahedral (644 cm<sup>-1</sup>), and the W–O deformation mode (562 cm<sup>-1</sup>) [10,31–33]. After addition of the additives, besides those from WO<sub>3</sub>, some new bands appear, such as a series of weak bands at 1100–1600 cm<sup>-1</sup> attributed to the N–H, C–H, C–N, C–C, and aromatic C–C bonds due to the additives, as shown in Curve b–f. In addition, broad and strong bands at 3247, 3237, and 3206 cm<sup>-1</sup> occur corresponding to the stretching vibration of N–H of DA, TA and PEA for Curve b, d and f,

respectively. DA, TA and PEA all contain an amino group but different numbers of hydroxyl groups. The DA molecule has two adjacent hydroxyl groups that can preferentially bind tungsten strongly via the deprotonated O, O' sites and the interaction between the amino group and PTA may be very limited. The TA molecule has only one hydroxyl group to link tungsten, and the PEA molecule has no hydroxyl group and thus may only form hydrogen bonding or an electrostatic interaction between NH<sub>2</sub> or NH<sub>3</sub><sup>+</sup> groups on PEA and O atoms on the xerogel, which consequently causes these stretching vibration bands of N–H to shift to lower frequencies. Therefore, it is inferred that the interaction order, in which the additives are preferentially bonded with the xerogel, may be the catechol hydroxyl groups, hydroxyl group, and aliphatic side chain (NH<sub>2</sub> or NH<sub>3</sub><sup>+</sup>). Certainly, these newly emerging peaks imply the coexistence of tungsten oxide and organic additives. The superposition of the bending vibration of water molecules in WO<sub>3</sub> xerogel and O–H and/or N–H bonds in complex xerogels makes the peaks stronger and wider, which shift to lower wavenumbers (from 1629 cm<sup>-1</sup> to about 1620 cm<sup>-1</sup>) owing to the interaction of the additives and PTA. Moreover, after the addition of DA and CA into the PTA sol, both the terminal W=O peaks of these two complex xerogels move in the lower wavenumber direction (from 975 cm<sup>-1</sup> for the WO<sub>3</sub> xerogel to 970 cm<sup>-1</sup> for WO<sub>3</sub>/DA and WO<sub>3</sub>/CA xerogels) because the catechol hydroxyl groups of DA and CA are bidentate, showing a relatively strong complexation with W atoms, while the W=O peak positions of other complex xerogels containing monodentate change little. The peaks of the WO<sub>3</sub> complex xerogels corresponding to the stretching vibrations of W–O–W bands and the W–O deformation mode downshift obviously from 644 cm<sup>-1</sup> to about 630 cm<sup>-1</sup> and from 562 cm<sup>-1</sup> to about 550 cm<sup>-1</sup>, respectively, further verifying the formation of the complexes by the interactions between phenolic hydroxyl groups or amino groups (NH<sub>2</sub> or NH<sub>3</sub><sup>+</sup>) of the additives and W or O species of PTA. In addition, oxidation products of the additives containing phenolic hydroxyl groups (DA, CA, TA and Ph), such as quinone, were also found according to the weak bands at about 1700–1770 cm<sup>-1</sup>, meaning some of the phenolic hydroxyl groups were also oxidized slightly during the complexation process.

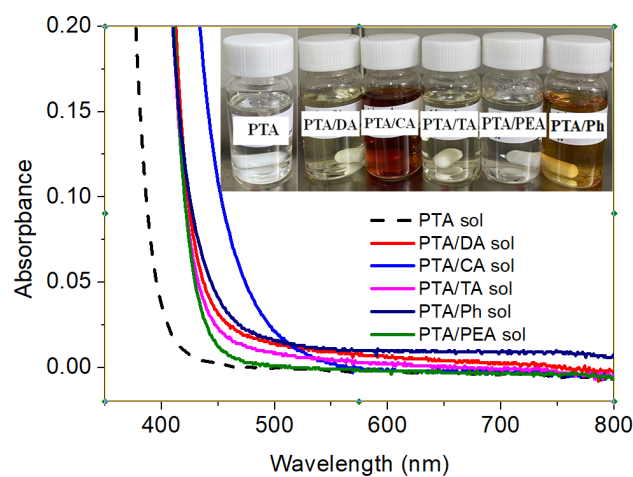


**Figure 2.** UV-Vis absorption spectra of the PTA, PTA/DA, PTA/CA, PTA/TA, PTA/Ph, and PTA/PEA sols. The inset showing the photos of these sols.

After spin-coating of all the PTA and complex sols and then annealing at 300 °C for 2 h, the obvious decrease in the intensity or even disappearance of W=O and W–O–O–W absorption bands of the WO<sub>3</sub>-300 °C and modified films (Curve a-f in Figure 3B) can be attributed to the aging and condensation of WO<sub>6</sub> octahedral units at their corners to form a W–O–W network [33]. Furthermore, the loss of structural and absorbed water when heating at 300 °C results in the weakening of the bands at ~3500 cm<sup>-1</sup> and ~1630 cm<sup>-1</sup>. The absorbance bands at ~1400 cm<sup>-1</sup> can be ascribed to the W–OH bending vibration. At the same time, the weak bands attributed to the additives at 1100–1600 cm<sup>-1</sup> disappear due to the burning off organic additives after annealing at 300 °C for 2 h. On the other hand,

the intensity increase in the W–O–W band and well-defined double bands at  $813\text{ cm}^{-1}$  and  $758\text{ cm}^{-1}$  for the  $\text{WO}_3\text{-}300\text{ }^\circ\text{C}$  film (Curve a in Figure 3B) reveal the crystalline structure of  $\text{WO}_3$ . In contrast, the absence of the double bands and the obvious broad bands at  $600\text{--}670\text{ cm}^{-1}$  in Curve b–f indicate that the dominant structure of the films modified by the additives is different from crystalline one of the  $\text{WO}_3\text{-}300\text{ }^\circ\text{C}$  film.

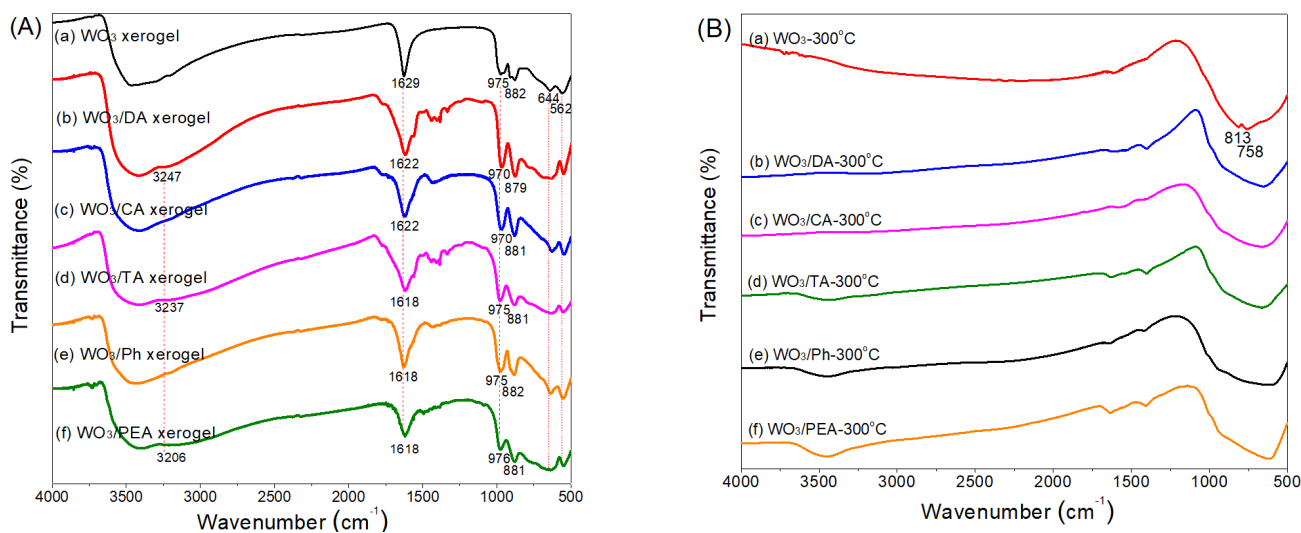


**Figure 3.** (A) FTIR spectra of (a)  $\text{WO}_3$ , (b)  $\text{WO}_3/\text{DA}$ , (c)  $\text{WO}_3/\text{CA}$ , (d)  $\text{WO}_3/\text{TA}$ , (e)  $\text{WO}_3/\text{Ph}$  and (f)  $\text{WO}_3/\text{PEA}$  xerogels, and (B) FTIR spectra of (a)  $\text{WO}_3\text{-}300\text{ }^\circ\text{C}$ , (b)  $\text{WO}_3/\text{DA}\text{-}300\text{ }^\circ\text{C}$ , (c)  $\text{WO}_3/\text{CA}\text{-}300\text{ }^\circ\text{C}$ , (d)  $\text{WO}_3/\text{TA}\text{-}300\text{ }^\circ\text{C}$ , (e)  $\text{WO}_3/\text{Ph}\text{-}300\text{ }^\circ\text{C}$  and (f)  $\text{WO}_3/\text{PEA}\text{-}300\text{ }^\circ\text{C}$  films.

The structures and morphologies of the  $\text{WO}_3$  films were studied by electron microscopes. Figure S1 shows FESEM images of the  $\text{WO}_3\text{-}300\text{ }^\circ\text{C}$  and modified films, revealing that all the films present relatively smooth, uniform and close-packed surfaces.

The TEM images of all the films can be seen from Figure 4. Different from the  $\text{WO}_3\text{-}300\text{ }^\circ\text{C}$  film exhibiting uniform polycrystalline structure (Figure 4A), the modified films show that  $\text{WO}_3$  nanocrystals are uniformly separated from each other and distributed in an amorphous  $\text{WO}_3$  matrix (Figure 4B–F). The amorphous matrix surrounding the  $\text{WO}_3$  nanocrystals may act as ion transport channels and increase reactive active sites during the EC process, which is beneficial for the diffusion of the electrolyte into the nanocrystals [10] and the improvement of the optical contrast and switching response. Meanwhile, the amorphous phase in the nanocrystal-embedded films may also serve as buffer layers to accommodate the volume change produced by ion insertion/extraction [18] and avoid bond breakage during electrochemical cycling. The amorphous and nanocrystalline regions were uniformly distributed, which may decrease the stress concentration and inhibit erosion produced by high local stress, contributing to high cycling stability [23]. According to Figure 4B–F, the estimated particle sizes of the crystalline grains increase gradually in the range of from about 5 to 20 nm in the following order:  $\text{WO}_3/\text{DA}\text{-}300\text{ }^\circ\text{C}$ ,  $\text{WO}_3/\text{CA}\text{-}300\text{ }^\circ\text{C}$ ,  $\text{WO}_3/\text{TA}\text{-}300\text{ }^\circ\text{C}$ ,  $\text{WO}_3/\text{Ph}\text{-}300\text{ }^\circ\text{C}$  and  $\text{WO}_3/\text{PEA}\text{-}300\text{ }^\circ\text{C}$ . Due to the high coordination ability of catechol hydroxyl groups on metals, the strong complexation of catechol additives (such as DA and CA) can limit the size of colloidal particles and destroy the structure order of particles to a certain extent, which results in the formation of more uniform and finer nanocrystals distributed in an amorphous matrix after heat treatment at  $300\text{ }^\circ\text{C}$ . Compared with CA, DA also contains  $\text{NH}_3^+$ , which can help PTA colloidal particles to better disperse in colloid and thus stabilize colloid solution. However, the complexation ability of monodentate additives (TA, Ph and PEA) is slightly poor, especially for PEA containing only one amino group without hydroxyl group, resulting in the formation of relatively large and heterogeneous nanocrystals after annealing. Different numbers and types of functional groups in the additives may have different effects on the microstructure

and morphology of the films, therefore, and will ultimately result in a large difference in the properties of the films including EC property. Moreover, according to TEM images, clear lattice fringes of nanocrystals can be seen for the  $\text{WO}_3$ -300 °C and modified films, and the lattice spacing values (3.83, 3.77, and 3.66 Å) perfectly fit monoclinic  $\text{WO}_3$  (JCPDS 43-1035), corresponding to the d-spacing of (002), (020), and (200) planes.

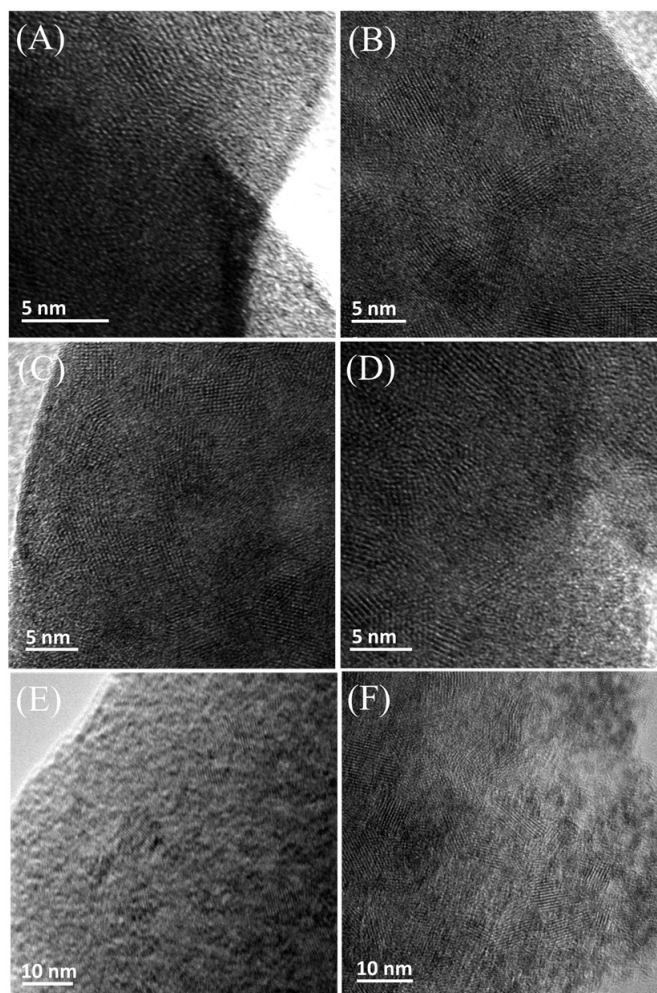


**Figure 4.** TEM images of (A)  $\text{WO}_3$ -300 °C, (B)  $\text{WO}_3/\text{DA}$ -300 °C, (C)  $\text{WO}_3/\text{CA}$ -300 °C, (D)  $\text{WO}_3/\text{TA}$ -300 °C, (E)  $\text{WO}_3/\text{Ph}$ -300 °C, and (F)  $\text{WO}_3/\text{PEA}$ -300 °C films.

Figure 5 shows XRD patterns of ITO glass,  $\text{WO}_3$ -300 °C,  $\text{WO}_3/\text{DA}$ -300 °C,  $\text{WO}_3/\text{CA}$ -300 °C,  $\text{WO}_3/\text{TA}$ -300 °C,  $\text{WO}_3/\text{Ph}$ -300 °C, and  $\text{WO}_3/\text{PEA}$ -300 °C films coated on ITO glass. After annealing at 300 °C for 2 h, the  $\text{WO}_3$ -300 °C film displays several relatively intense and distinct diffraction peaks at  $2\theta = 23.2, 23.7, 24.4$  and  $34.2^\circ$  in Curve b corresponding to (002), (020), (200) and (202) planes, respectively, indexed to the monoclinic crystalline  $\text{WO}_3$  (JCPDS Card No.43-1035). However, for the modified films (Curve c-g), only weak and broad humps appear in the  $2\theta$  region from  $20^\circ$  to  $30^\circ$  in addition to several characteristic peaks of the ITO substrate, as shown in Curve a. During the preparation of the modified films, the additives may inhibit crystal growth, causing the generation of the small  $\text{WO}_3$  nanocrystals embedded in an amorphous matrix, which is in agreement with the FTIR and TEM results, which broaden and weaken the diffraction peaks. Therefore, it is difficult to observe distinct diffraction peaks [30,34].

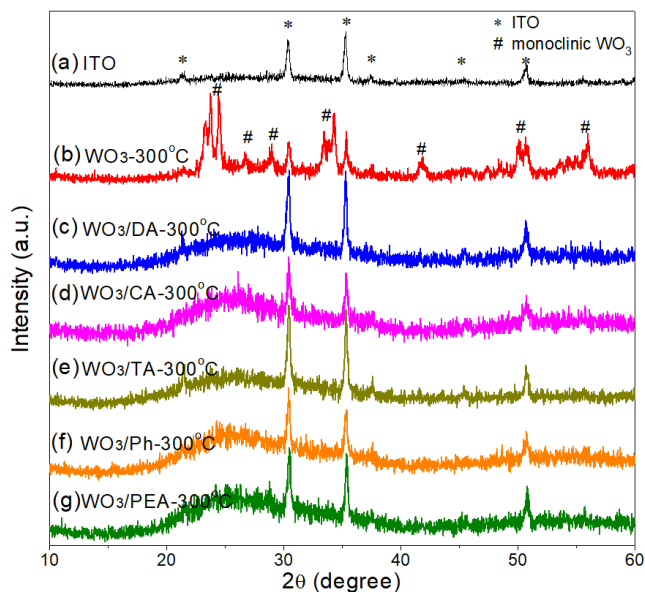


**Figure 5.** X-ray diffraction (XRD) patterns of (a) ITO glass, (b)  $\text{WO}_3$ -300 °C, (c)  $\text{WO}_3/\text{DA}$ -300 °C, (d)  $\text{WO}_3/\text{CA}$ -300 °C, (e)  $\text{WO}_3/\text{TA}$ -300 °C, (f)  $\text{WO}_3/\text{Ph}$ -300 °C, and (g)  $\text{WO}_3/\text{PEA}$ -300 °C films.

### 3.2. Electrochemical Properties of the Modified $\text{WO}_3$ Films

The electrochemical properties of the films during ion insertion/extraction were studied by using CV. Figure 6A displays the CV curves of the  $\text{WO}_3$ -300 °C and modified  $\text{WO}_3$  films tested at a scan rate of  $100 \text{ mV s}^{-1}$  between  $-1.0$  and  $+1.0$  V. For all the films, the CV curves are similar in shape, but the modified films exhibit a higher peak current density and CV integral area than the  $\text{WO}_3$ -300 °C film, and the order of the modified films from high to low is roughly  $\text{WO}_3/\text{DA}$ -300 °C,  $\text{WO}_3/\text{CA}$ -300 °C,  $\text{WO}_3/\text{TA}$ -300 °C,  $\text{WO}_3/\text{Ph}$ -300 °C and  $\text{WO}_3/\text{PEA}$ -300 °C. Therefore, the modified films have more electrochemical active mass and higher ion/electron storage capacity, that is, more ions/electrons are involved at the interface between the films and electrolyte than the  $\text{WO}_3$ -300 °C film, and thus, it is deduced that the modified films will show better EC performances due to the nanocrystal-embedded amorphous structure.

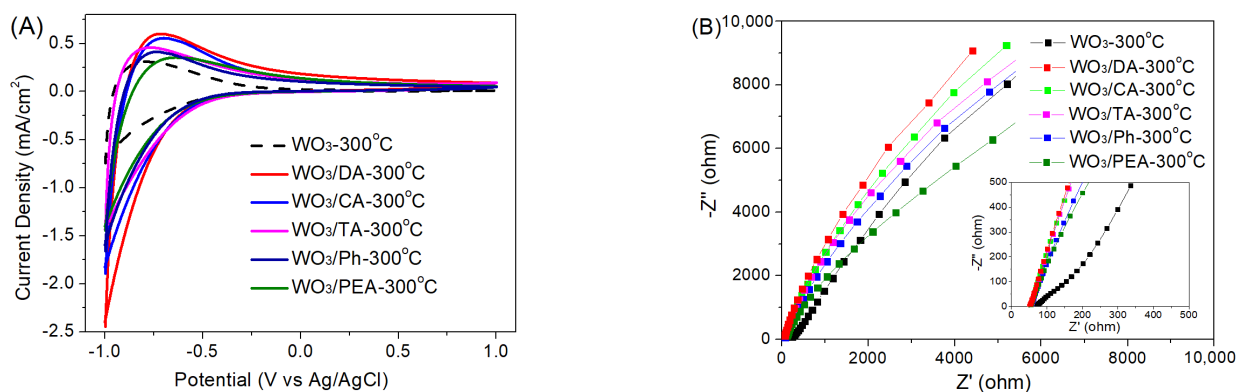


**Figure 6.** (A) CV curves tested at a scan rate of  $100 \text{ mV s}^{-1}$  between  $-1.0$  and  $+1.0$  V and (B) Nyquist plots of the  $\text{WO}_3$ -300 °C,  $\text{WO}_3/\text{DA}$ -300 °C,  $\text{WO}_3/\text{CA}$ -300 °C,  $\text{WO}_3/\text{TA}$ -300 °C,  $\text{WO}_3/\text{Ph}$ -300 °C and  $\text{WO}_3/\text{PEA}$ -300 °C films in 1 mol/L  $\text{LiClO}_4/\text{PC}$  at frequency from 100 kHz to 10 mHz using a perturbation amplitude of 10 mV at the potential of 0 V.

Electrochemical impedance spectroscopy (EIS) was applied to further investigate the electrochemical behaviors of the modified  $\text{WO}_3$  films and provided information on the interfaces of charge transfer and ion diffusion. The Nyquist plots of the  $\text{WO}_3$ -300 °C



and modified WO<sub>3</sub> films can be seen in Figure 6B. Compared with the WO<sub>3</sub>-300 °C, the modified WO<sub>3</sub> films (especially WO<sub>3</sub>/DA-300 °C) exhibit smaller intercepts of the curves at the X-axis and depressed arc diameters in the high-frequency region (the inset of Figure 6B) and higher slopes in the low-frequency region (except WO<sub>3</sub>/PEA-300 °C), meaning lower series resistance and charge-transfer resistance and a higher diffusion rate of Li<sup>+</sup> ion for ion insertion into and extraction from the films [35–37]. The results indicate that the nanocrystal-embedded amorphous phase structure of the modified films is more beneficial to both Li<sup>+</sup> ion diffusion and charge transfer compared with the compact polycrystalline structure of WO<sub>3</sub>-300 °C.

### 3.3. EC properties of the Modified WO<sub>3</sub> Films

The EC process of WO<sub>3</sub> films involves the double injection/extraction of cations and electrons into/from the films and the color switches between blue and transparent. EC properties of the pure WO<sub>3</sub>-300 °C and modified films were tested and compared as shown in Figure 7 and Table 1. Transmittance contrast or modulation,  $\Delta T$ , is defined as the difference in the transmittance between the bleached and the colored states at a certain wavelength. According to UV-vis transmittance spectra (Figure 7A–F),  $\Delta T$  values of the WO<sub>3</sub>-300 °C, WO<sub>3</sub>/DA-300 °C, WO<sub>3</sub>/CA-300 °C, WO<sub>3</sub>/TA-300 °C, WO<sub>3</sub>/Ph-300 °C and WO<sub>3</sub>/PEA-300 °C films at a wavelength of 720 nm are about 51, 75, 72, 66, 64, and 56%, respectively, as listed in Table 1. Compared with the pure WO<sub>3</sub>-300 °C film, all the modified WO<sub>3</sub> films possess much higher optical contrasts ( $\Delta T$ ) because the nanocrystal-embedded amorphous structure produced by the additives can provide more active sites and higher ion/electron storage capacity than the compact polycrystalline structure. Therefore, as we can see from the aforementioned test results related to the characterization and electrochemical properties, different numbers and types of functional groups in the additives may ultimately result in a large difference in the EC properties of the films by changing the microstructure and morphology of the films. In other words, the addition of the additives with more hydroxyl groups produces the modified WO<sub>3</sub> films with better performances.

Coloration efficiency ( $CE$ ) is defined as the change in optical density ( $\Delta OD$ ) measured at a certain wavelength ( $\lambda$ ) per unit charge ( $Q$ ) inserted into or extracted from the EC films, namely,  $CE = \Delta OD(\lambda)/(Q/A) = \log(T_b/T_c)/q$  [38], where  $q$  is the charge density (injected/ejected charge  $Q$  per unit electrode area  $A$ ), and  $T_b$  and  $T_c$  represent the transmittances in the bleached and colored states. Coloration efficiency is also an important characteristic parameter for evaluating EC performance. The coloration efficiency values were calculated to be 66, 90, 85, 81, 77 and 70 cm<sup>2</sup> C<sup>-1</sup> for the WO<sub>3</sub>-300 °C, WO<sub>3</sub>/DA-300 °C, WO<sub>3</sub>/CA-300 °C, WO<sub>3</sub>/TA-300 °C, WO<sub>3</sub>/Ph-300 °C and WO<sub>3</sub>/PEA-300 °C films, respectively, as listed in Table 1. The much higher coloration efficiency values of the modified WO<sub>3</sub> films than that of WO<sub>3</sub>-300 °C film can be ascribed to their more efficient Li<sup>+</sup> ion diffusion and charge transfer in the nanocrystal-embedded amorphous structure. In general, high coloration efficiency provides a large optical contrast with a small charge insertion or extraction, which is beneficial to improving the cycle life of the EC materials, just as our previous work proved that the WO<sub>3</sub>/DA-300 °C film displays excellent stability up to 35,000 cycles [23]. All the modified films exhibit the unique nanocrystal-embedded amorphous structure as shown in TEM images, which consequently help to greatly improve cycling stability of all the modified films.

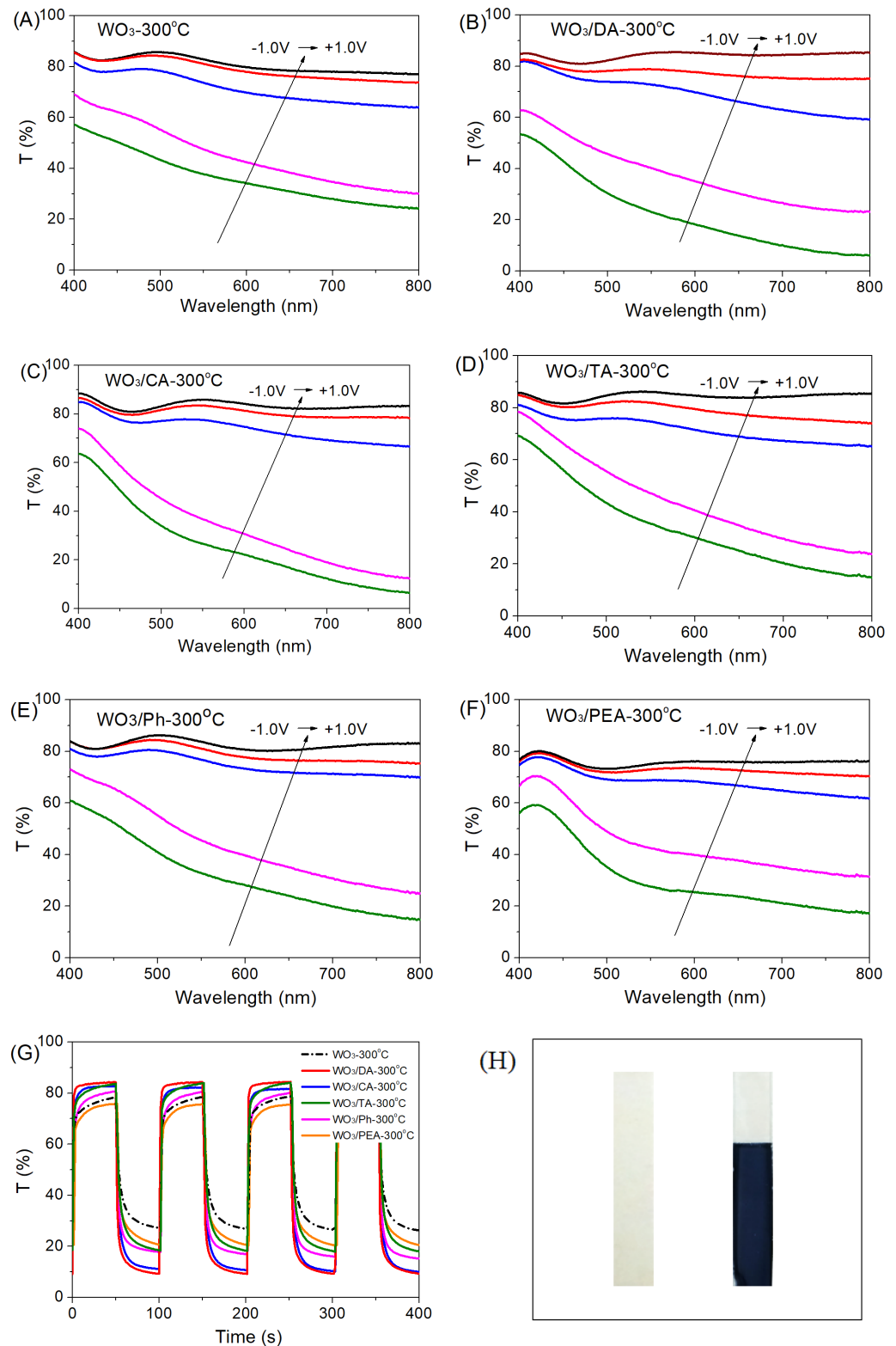


**Figure 7.** UV-vis transmittance spectra at different potentials of (A) pure  $\text{WO}_3$ -300 °C, (B)  $\text{WO}_3/\text{DA}$ -300 °C, (C)  $\text{WO}_3/\text{CA}$ -300 °C, (D)  $\text{WO}_3/\text{TA}$ -300 °C, (E)  $\text{WO}_3/\text{Ph}$ -300 °C, and (F)  $\text{WO}_3/\text{PEA}$ -300 °C films at the potentials of  $-1.0$ ,  $-0.8$ ,  $+0.5$ ,  $+0.8$  and  $+1.0$  V, as shown in green, violet, blue, red and black lines, respectively, (G) switching curve comparison between the  $\text{WO}_3$ -300 °C,  $\text{WO}_3/\text{DA}$ -300 °C,  $\text{WO}_3/\text{CA}$ -300 °C,  $\text{WO}_3/\text{TA}$ -300 °C,  $\text{WO}_3/\text{Ph}$ -300 °C, and  $\text{WO}_3/\text{PEA}$ -300 °C films at  $\lambda_{720\text{nm}}$  ( $+1.0$  V/ $-1.0$  V, 100 s per cycle), and (H) the photo of the  $\text{WO}_3/\text{DA}$ -300 °C films in the bleached and colored states respectively.

**Table 1.** EC properties of the WO<sub>3</sub>-300 °C, WO<sub>3</sub>/DA-300 °C, WO<sub>3</sub>/CA-300 °C, WO<sub>3</sub>/TA-300 °C, WO<sub>3</sub>/Ph-300 °C and WO<sub>3</sub>/PEA-300 °C films at λ<sub>720nm</sub>.

The Films	ΔT <sup>1</sup> (%)	ΔT <sup>2</sup> (%)	CE (cm <sup>2</sup> C <sup>-1</sup> )	Bleaching Time <sup>2</sup> (s)	Coloration Time <sup>2</sup> (s)
WO <sub>3</sub> -300 °C	51 ± 1	52 ± 1	66 ± 1	10 ± 1	15 ± 1
WO <sub>3</sub> /DA-300 °C	75 ± 1	75 ± 1	90 ± 1	3 ± 1	7 ± 1
WO <sub>3</sub> /CA-300 °C	72 ± 1	71 ± 1	85 ± 1	5 ± 1	10 ± 1
WO <sub>3</sub> /TA-300 °C	66 ± 1	66 ± 1	81 ± 1	6 ± 1	13 ± 1
WO <sub>3</sub> /Ph-300 °C	64 ± 1	63 ± 1	77 ± 1	9 ± 1	9 ± 1
WO <sub>3</sub> /PEA-300 °C	56 ± 1	55 ± 1	70 ± 1	9 ± 1	15 ± 1

<sup>1</sup> Obtained from UV-Vis transmittance spectra in Figure 7A–F; <sup>2</sup> Obtained from switching curves in Figure 7G.

The switching times, namely coloration and bleaching times, mean the times required for a 90% change in the transmittance contrast during the coloring/bleaching processes, which have been measured from switching curves of the films in Figure 7G and can be seen in Table 1. The switching times for the WO<sub>3</sub>/DA-300 °C film are 10 s for bleaching and 15 s for coloration, while the switching times for the modified WO<sub>3</sub> film are almost all less than them, indicating that using the additives can accelerate the dynamic response of WO<sub>3</sub> films. The reason is that the modified WO<sub>3</sub> films with nanocrystal-embedded amorphous structure possess a much shorter diffusion length of ions due to a larger amorphous region and easier access of a larger amount of Li<sup>+</sup> ions than the WO<sub>3</sub>-300 °C film with a polycrystalline structure, which can consequently speed up the ion diffusion and charge transfer. Of all the films, the WO<sub>3</sub>/DA-300 °C film shows the shortest switching time (3 s for bleaching and 7 s for coloration), because it possesses the smallest nanocrystals uniformly distributed in an amorphous WO<sub>3</sub> matrix which may act as ion transport channels and increase reactive active sites during EC process, which is beneficial for the diffusion of the electrolyte into the nanocrystals and the speeding up of the switching response. For most films, the bleaching times are less than the coloration times, showing that the double extraction of cations and electrons from the films is easier and faster than injection into the films.

As we all know, the structure and morphology of WO<sub>3</sub> films greatly affects EC performance, and amorphous and crystalline WO<sub>3</sub> films exhibit quite different EC performances from each other [39]. In this study, the introduction of the additives into the precursor PTA sol and the application of an appropriate annealing process promote the formation of nanocrystal-embedded amorphous structure having the merits of both amorphous and crystalline WO<sub>3</sub> films. All the modified films possess higher EC properties than the pure WO<sub>3</sub> polycrystalline film, roughly in descending order: the WO<sub>3</sub>/DA-300 °C, WO<sub>3</sub>/CA-300 °C, WO<sub>3</sub>/TA-300 °C, WO<sub>3</sub>/Ph-300 °C and WO<sub>3</sub>/PEA-300 °C films. The strong complexation ability (with W atoms) of DA and CA bidentate additives containing catechol hydroxyl groups limits the size of complex colloidal particles and destroys the structure order of particles to a certain extent, resulting in the formation of more uniform and finer nanocrystals surrounded with an amorphous matrix after heat treatment. On the other hand, among them, DA has the best effect in enhancing the EC properties of the films because it also contains NH<sub>3</sub><sup>+</sup> in addition to catechol hydroxyl groups, which can be better dispersed in colloid and thus stabilize colloid solution. TA, PEA and Ph, however, are monodentate additives and show slightly poor complexation ability, resulting in the formation of relatively large and uneven nanocrystals. Especially, PEA contains only one amine group without a hydroxyl group, and the film modified by PEA shows relatively poorer EC performance than other modified films.

#### 4. Conclusions

In summary, a series of organic small molecules (DA, CA, TA, Ph and PEA) containing different numbers of hydroxyl and amino groups were added to the PTA sols as structure-directing additives, and a variety of modified WO<sub>3</sub> films were consequently

prepared by a simple and low-cost complexation-assisted sol–gel method. Compared with the pure  $\text{WO}_3$  polycrystalline film, all the modified films combine the advantages of nanocrystalline and amorphous phases and show higher EC properties owing to the unique nanocrystal-embedded amorphous structure. It is worth noting that the additives with different numbers and types of functional groups show different interactions with PTA sol, which affect the size, shape and stability of the complex colloidal particles and consequently change the structures and morphologies of the  $\text{WO}_3$  films from a polycrystalline to nanocrystal-embedded amorphous structure with different grain sizes, finally improving the electrochemical and EC properties of the modified  $\text{WO}_3$  films in different degrees. The additives, in order of their interactions with the sol, are DA, CA, TA, Ph and PEA, primarily depending on the number of hydroxyl groups followed by the number of amino group. Of all the additives, DA with catechol hydroxyl and amino groups shows the most positive effect, that is, the  $\text{WO}_3/\text{DA-300}^\circ\text{C}$  film exhibits the best EC performances.

Furthermore, the study indicates that the modified  $\text{WO}_3$  films with excellent EC properties prepared by a simple and low-cost complexation-assisted sol–gel method show great application potential for EC devices. The effects of more additives with other functional groups on the microstructure, morphology, and thus EC properties of the  $\text{WO}_3$  films should be further studied in the future to reveal the relationship between structure and performance of the  $\text{WO}_3$  films and further improve the complexation-assisted sol–gel method.

**Supplementary Materials:** The following supporting information can be downloaded at: <https://www.mdpi.com/article/10.3390/ma16072681/s1>, Figure S1: FESEM images of (A)  $\text{WO}_3\text{-300}^\circ\text{C}$ , (B)  $\text{WO}_3/\text{DA-300}^\circ\text{C}$ , (C)  $\text{WO}_3/\text{CA-300}^\circ\text{C}$ , (D)  $\text{WO}_3/\text{TA-300}^\circ\text{C}$ , (E)  $\text{WO}_3/\text{Ph-300}^\circ\text{C}$ , and (F)  $\text{WO}_3/\text{PEA-300}^\circ\text{C}$  films.

**Author Contributions:** Conceptualization, D.Z.; methodology, D.Z. and Z.T.; validation, H.X. and J.S.; preparation, D.Z.; characterization, F.C.; writing—original draft preparation, D.Z.; writing—review and editing, F.C.; supervision, D.Z. All authors have read and agreed to the published version of the manuscript.

**Funding:** This research was funded by the Chongqing Research Program of Basic Research and Frontier Technology (cstc2019jcyj-msxmX0510) and the Research Project of Yangtze Normal University (2017KYQD39).

**Institutional Review Board Statement:** Not applicable.

**Informed Consent Statement:** Not applicable.

**Data Availability Statement:** All data are available from the corresponding author.

**Acknowledgments:** The authors would like to thank Qihuang Deng for the XRD characterization. This work was financially supported by the Chongqing Research Program of Basic Research and Frontier Technology (cstc2019jcyj-msxmX0510) and the Research Project of Yangtze Normal University (2017KYQD39).

**Conflicts of Interest:** The authors declare no conflict of interest.

## References

1. Zhang, Y.; Liang, X.; Jiang, T.; Liu, H.; Fu, Y.; Zhang, D.; Geng, Z. Amorphous/crystalline  $\text{WO}_3$  dual phase laminated films: Fabrication, characterization and evaluation of their electrochromic performance for smart window applications. *Sol. Energy Mater. Sol. Cells* **2022**, *244*, 111820. [[CrossRef](#)]
2. Luo, Y.; Jin, H.; Lu, Y.; Zhu, Z.; Dai, S.; Huang, L.; Zhuang, X.; Liu, K.; Huang, L. Potential Gradient-Driven Fast-Switching Electrochromic Device. *ACS Energy Lett.* **2022**, *7*, 1880–1887. [[CrossRef](#)]
3. Niklasson, G.A.; Granqvist, C.G. Electrochromics for smart windows: Thin films of tungsten oxide and nickel oxide, and devices based on these. *J. Mater. Chem.* **2007**, *17*, 127–156. [[CrossRef](#)]
4. Wang, J.; Zhang, L.; Yu, L.; Jiao, Z.; Xie, H.; Lou, X.W.; Sun, X.W. A bi-functional device for self-powered electro-chromic window and self-rechargeable transparent battery applications. *Nat. Commun.* **2014**, *5*, 4921. [[CrossRef](#)]
5. Thakur, V.K.; Ding, G.Q.; Ma, J.; Lee, P.S.; Lu, X.H. Hybrid Materials and Polymer Electrolytes for Electrochromic Device Applications. *Adv. Mater.* **2012**, *24*, 4071–4096.

6. Wu, C.-L.; Wang, C.-K.; Lin, C.-K.; Wang, S.-C.; Huang, J.-L. Electrochromic properties of nanostructured tungsten oxide films prepared by surfactant-assisted sol–gel process. *Surf. Coat. Technol.* **2013**, *231*, 403–407. [[CrossRef](#)]
7. Gesheva, K.; Szekeres, A.; Ivanova, T. Optical properties of chemical vapor deposited thin films of molybdenum and tungsten based metal oxides. *Sol. Energy Mater. Sol. Cells* **2003**, *76*, 563–576. [[CrossRef](#)]
8. Subrahmanyam, A.; Karupphasamy, A. Optical and electrochromic properties of oxygen sputtered tungsten oxide (WO<sub>3</sub>) thin films. *Sol. Energy Mater. Sol. Cells* **2007**, *91*, 266–274. [[CrossRef](#)]
9. Baek, Y.; Yong, K. Controlled Growth and Characterization of Tungsten Oxide Nanowires Using Thermal Evaporation of WO<sub>3</sub> Powder. *J. Phys. Chem. C* **2007**, *111*, 1213–1218. [[CrossRef](#)]
10. Lin, F.; Cheng, J.; Engtrakul, C.; Dillon, A.C.; Nordlund, D.; Moore, R.G.; Weng, T.-C.; Williams, S.K.R.; Richards, R.M. In situ crystallization of high performing WO<sub>3</sub>-based electrochromic materials and the importance for durability and switching kinetics. *J. Mater. Chem.* **2012**, *22*, 16817–16823. [[CrossRef](#)]
11. Gillaspie, D.T.; Tenent, R.C.; Dillon, A.C. Metal-oxide films for electrochromic applications: Present technology and future directions. *J. Mater. Chem.* **2010**, *20*, 9585–9592. [[CrossRef](#)]
12. Cronin, J.; Tarico, D.; Tonazzi, J.; Agrawal, A.; Kennedy, S. Microstructure and properties of sol-gel deposited WO<sub>3</sub> coatings for large area electrochromic windows. *Sol. Energy Mater. Sol. Cells* **1993**, *29*, 371–386. [[CrossRef](#)]
13. Taylor, D.J.; Cronin, J.P.; Allard, L.F.; Birnie, D.P. Microstructure of laser-fired, sol-gel-derived tungsten oxide films. *Chem. Mater.* **1996**, *8*, 1396–1401.
14. Shchegolkov, A.V.; Jang, S.-H.; Shchegolkov, A.V.; Rodionov, Y.V.; Sukhova, A.O.; Lipkin, M.S. A Brief Overview of Electrochromic Materials and Related Devices: A Nanostructured Materials Perspective. *Nanomaterials* **2021**, *11*, 2376. [[CrossRef](#)]
15. Wang, W.; Pang, Y.; Hodgson, S.N.B. Preparation, characterisation and electrochromic property of mesostructured tungsten oxide films via a surfactant templated sol–gel process from tungstic acid. *J. Sol-Gel Sci. Technol.* **2010**, *54*, 19–28. [[CrossRef](#)]
16. Badilescu, S.; Ashrit, P.V. Study of sol-gel prepared nanostructured WO<sub>3</sub> thin films and composites for electro-chromic applications. *Solid State Ion.* **2003**, *158*, 187–197. [[CrossRef](#)]
17. Baeck, S.H.; Choi, K.S.; Jaramillo, T.F.; Stucky, G.D.; McFarland, E.W. Enhancement of photocatalytic and electrochromic properties of electrochemically fabricated mesoporous WO<sub>3</sub> thin films. *Adv. Mater.* **2003**, *15*, 1269. [[CrossRef](#)]
18. Fang, Y.; Sun, X.; Cao, H. Influence of PEG additive and annealing temperature on structural and electrochromic properties of sol–gel derived WO<sub>3</sub> films. *J. Sol-Gel Sci. Technol.* **2011**, *59*, 145–152. [[CrossRef](#)]
19. He, J.; Yang, X.; Evans, D.; Duan, X. New methods to remove organic templates from porous materials. *Mater. Chem. Phys.* **2003**, *77*, 270–275. [[CrossRef](#)]
20. Cronin, J.P.; Tarico, D.J.; Agrawal, A.; Zhang, R.L. Method for Depositing High Performing Electrochromic Layers. U.S. Patent 5277986, 11 January 1994.
21. Deepa, M.; Saxena, T.; Singh, D.; Sood, K.; Agnihotry, S. Spin coated versus dip coated electrochromic tungsten oxide films: Structure, morphology, optical and electrochemical properties. *Electrochim. Acta* **2006**, *51*, 1974–1989. [[CrossRef](#)]
22. Shi, Y.; Sun, M.; Zhang, Y.; Cui, J.; Wang, Y.; Shu, X.; Qin, Y.; Tan, H.H.; Liu, J.; Wu, Y. Structure modulated amorphous/crystalline WO<sub>3</sub> nanoporous arrays with superior electrochromic energy storage performance. *Sol. Energy Mater. Sol. Cells* **2020**, *212*, 110579. [[CrossRef](#)]
23. Zhou, D.; Che, B.; Kong, J.; Lu, X. A nanocrystalline tungsten oxide electrochromic coating with excellent cycling stability prepared via a complexation-assisted sol–gel method. *J. Mater. Chem. C* **2016**, *4*, 8041–8051. [[CrossRef](#)]
24. Wang, Z.; Zou, Y.; Li, Y.; Cheng, Y. Metal-Containing Polydopamine Nanomaterials: Catalysis, Energy, and Theranostics. *Small* **2020**, *16*, 1907042.
25. Nielson, A.J.; Griffith, W.P. Complexes of osmium(VI) with catechol and substituted catechols. *J. Chem. Soc. Dalton Trans.* **1978**, 1501–1506. [[CrossRef](#)]
26. Griffith, W.P.; Pumphrey, C.A.; Rainey, T.A. Catecholato complexes of ruthenium, iridium, rhenium, molybdenum, and tungsten. *J. Chem. Soc.-Dalton Trans.* **1986**, 1125–1128. [[CrossRef](#)]
27. Elhendawy, A.M.; Griffith, W.P.; Pumphrey, C.A. Complexes of osmium, uranium, molybdenum, and tungsten with the catechol amines adrenaline, noradrenaline, dopamine, dopa, and iso-proterenol. *J. Chem. Soc.-Dalton Trans.* **1988**, 1817–1821. [[CrossRef](#)]
28. Urdaneta, I.; Keller, A.; Atabek, O.; Palma, J.L.; Finkelstein-Shapiro, D.; Tarakeshwar, P.; Mujica, V.; Calatayud, M. Dopamine Adsorption on TiO<sub>2</sub> Anatase Surfaces. *J. Phys. Chem. C* **2014**, *118*, 20688–20693.
29. Kleiman-Shwarsctein, A.; Laursen, A.B.; Cavalca, F.; Tang, W.; Dahl, S.; Chorkendorff, I. A general route for RuO<sub>2</sub> deposition on metal oxides from RuO<sub>4</sub>. *Chem. Commun.* **2012**, *48*, 967–969. [[CrossRef](#)]
30. Valverde-Aguilar, G.; Prado-Prone, G.; Vergara-Aragon, P.; Garcia-Macedo, J.; Santiago, P.; Rendon, L. Photoconductivity studies on nanoporous TiO<sub>2</sub>/dopamine films prepared by sol-gel method. *Appl. Phys. A-Mater. Sci. Process.* **2014**, *116*, 1075–1084.
31. Daniel, M.F.; Desbat, B.; Lassegues, J.C.; Gerand, B.; Figlarz, M. Infrared and raman-study of WO<sub>3</sub> tungsten trioxides and WO<sub>3</sub>·XH<sub>2</sub>O tungsten trioxide hydrates. *J. Solid State Chem.* **1987**, *67*, 235–247.
32. Santato, C.; Odziemkowski, M.; Ulmann, M.; Augustynski, J. Crystallographically Oriented Mesoporous WO<sub>3</sub> Films: Synthesis, Characterization, and Applications. *J. Am. Chem. Soc.* **2001**, *123*, 10639–10649. [[CrossRef](#)] [[PubMed](#)]
33. Orel, B.; Groselj, N.; Krasovec, U.O.; Jese, R.; Georg, A. IR spectroscopic investigations of gasochromic and electrochromic sol-gel—Derived peroxotungstic acid/ormosil composite and crystalline WO<sub>3</sub> films. *J. Sol-Gel Sci. Technol.* **2002**, *24*, 5–22. [[CrossRef](#)]

34. Dalavi, D.S.; Devan, R.S.; Patil, R.A.; Patil, R.S.; Ma, Y.-R.; Sadale, S.B.; Kim, I.; Kim, J.-H.; Patil, P.S. Efficient electrochromic performance of nanoparticulate WO<sub>3</sub> thin films. *J. Mater. Chem. C* **2013**, *1*, 3722–3728. [[CrossRef](#)]
35. Huang, H.; Tian, J.; Zhang, W.; Gan, Y.; Tao, X.; Xia, X.; Tu, J. Electrochromic properties of porous NiO thin film as a counter electrode for NiO/WO<sub>3</sub> complementary electrochromic window. *Electrochim. Acta* **2011**, *56*, 4281–4286. [[CrossRef](#)]
36. Cong, S.; Tian, Y.; Li, Q.; Zhao, Z.; Geng, F. Single-Crystalline Tungsten Oxide Quantum Dots for Fast Pseudocapacitor and Electrochromic Applications. *Adv. Mater.* **2014**, *26*, 4260–4267. [[PubMed](#)]
37. Kondalkar, V.V.; Mali, S.S.; Kharade, R.R.; Khot, K.V.; Patil, P.B.; Mane, R.M.; Choudhury, S.; Patil, P.S.; Hong, C.K.; Kim, J.H.; et al. High performing smart electrochromic device based on honeycomb nanostructured h-WO<sub>3</sub> thin films: Hydrothermal assisted synthesis. *Dalton Trans.* **2015**, *44*, 2788–2800. [[CrossRef](#)]
38. Amb, C.M.; Dyer, A.L.; Reynolds, J.R. Navigating the Color Palette of Solution-Processable Electrochromic Polymers. *Chem. Mater.* **2011**, *23*, 397–415.
39. Quy, V.H.V.; Jo, I.-R.; Kang, S.-H.; Ahn, K.-S. Amorphous-crystalline dual phase WO<sub>3</sub> synthesized by pulsed-voltage electrodeposition and its application to electrochromic devices. *J. Ind. Eng. Chem.* **2021**, *94*, 264–271. [[CrossRef](#)]

**Disclaimer/Publisher's Note:** The statements, opinions and data contained in all publications are solely those of the individual author(s) and contributor(s) and not of MDPI and/or the editor(s). MDPI and/or the editor(s) disclaim responsibility for any injury to people or property resulting from any ideas, methods, instructions or products referred to in the content.